

Carbonic acid production in H₂O:CO₂ ices

UV photolysis vs. proton bombardment

P.A. Gerakines¹, M.H. Moore¹, and R.L. Hudson²

¹ Code 691, Astrochemistry Branch, NASA/Goddard Space Flight Center, Greenbelt, MD 20771, USA

² Department of Chemistry, Eckerd College, St. Petersburg, FL 33733, USA

Received 7 October 1999 / Accepted 6 March 2000

Abstract. We have the unique ability to perform ultraviolet photolysis (~ 10 eV photon⁻¹) and ion irradiation (0.8 MeV p⁺) in the same experimental set-up, with ices created under identical conditions. We present experiments that show the formation of carbonic acid (H₂CO₃) from H₂O:CO₂ ice mixtures exposed to either UV photons or high-energy protons. CO and CO₃ were also formed in these experiments. Results show that while H₂CO₃ is readily formed by p⁺ bombardment, its formation by UV photolysis is limited by the penetration of UV photons into the ice. H₂CO₃ production pathways are investigated. Intrinsic IR band strengths are determined for eight IR features of H₂CO₃. Implications for ices found in various astrophysical environments are discussed.

Key words: molecular data – molecular processes – methods: laboratory – comets: general – planets and satellites: general – ISM: molecules

1. Introduction

H₂O and CO₂ ices coexist in a variety of astrophysical environments. They are two of the most abundant molecules identified as constituents of icy grain mantles in the interstellar medium (Whittet et al. 1996). Moreover, recent observations obtained from the Infrared Space Observatory (ISO) indicate that a significant fraction of interstellar solid CO₂ exists in mixtures dominated by H₂O in both quiescent cloud and protostellar regions, with a ratio of total H₂O to total polar CO₂ ranging from 4 to 25 (Gerakines et al. 1999). For example, two-thirds of the total CO₂ toward the massive protostar NGC 7538 IRS9 exists in a polar ice at an abundance of 12.5 % relative to the total H₂O in this line of sight. The presence of CO₂ in cometary ices as a parent molecule is inferred from gas-phase observations of cometary comae. Relative to H₂O, CO₂ has an abundance of 6 % in comet Hale-Bopp (Crovisier 1998), and an upper limit of 7 % is given for Hyakutake (Bockelée-Morvan 1997). IR spectra of the icy Galilean satellites Europa, Ganymede, and Callisto show both H₂O and CO₂ ice features (Carlson et al. 1999; McCord et al.

1998). Also, H₂O and CO₂ are two of the molecules identified on the surfaces of Mars (Herr & Pimentel 1969; Larson & Fink 1972) and Triton (Quirico et al. 1999).

In this paper, we present the first comparison of UV-photolyzed and proton-irradiated ices in the same laboratory. The formation of H₂CO₃ by proton bombardment of H₂O:CO₂ ice mixtures has been shown previously in experiments by Moore & Khanna (1991), DelloRusso et al. (1993) and Brucato et al. (1997). However, there is a notable lack of H₂O:CO₂ UV photolysis data in the literature. The solitary experiment is found in a Ph.D. thesis (Zhao 1990), where an H₂O:CO₂ = 10:1 ice was photolyzed for six hours. The only analysis presented was focussed on the search for the formation of formaldehyde, which was not clearly identified in the ice spectra.

Our results represent not only the first comparison of the effects of UV photolysis and proton bombardment on H₂O:CO₂ ices, but also the first published study of H₂O:CO₂ photolysis itself. We show that CO and H₂CO₃ are the major products of H₂O:CO₂ = 1:1 mixtures exposed to either type of processing, and we compare the product yields in both cases with respect to the energy input to the ice. We also present measurements of carbonic acid's intrinsic IR band strengths, based on the UV photodissociation of crystalline H₂CO₃ at 18 K.

2. Experimental

The experimental system, ice preparation, and proton irradiation procedure have been described in detail by Hudson & Moore (1995) and Moore & Hudson (1998). In summary, gases are prepared inside a vacuum manifold and vapor-condensed onto a cold (T = 18 K) aluminum mirror suspended inside a stainless-steel high-vacuum chamber. Mixing ratios in the resultant ice are determined from the partial pressures inside the manifold before condensation. A schematic of the laboratory set-up is shown in Fig. 1. IR spectra (with a spectral range of 4000–400 cm⁻¹ and a resolution of 4 cm⁻¹) are taken by diverting the beam of an FTIR spectrometer (Mattson) toward the ice-covered mirror, where it passes through the ice before and after reflection at the ice-mirror interface.

Reagents used and their purities are as follows: H₂O (triply distilled, with a resistance greater than 10⁷ ohm cm), CO₂ (Matheson, 99.995 %), SF₆ (Pfaltz & Bauer, 99.8 %).

Send offprint requests to: P.A. Gerakines
(Perry.A.Gerakines@gssc.nasa.gov)

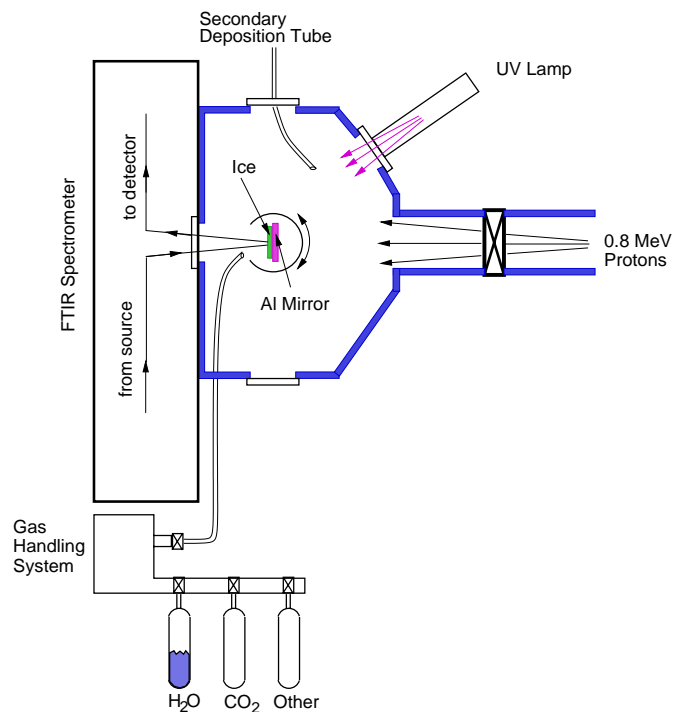


Fig. 1. Schematic of the laboratory set-up

Recently, a microwave-discharge hydrogen flow lamp (Ophos Instruments) that produces primarily Lyman- α photons ($\lambda = 121.6$ nm, $E = 10.2$ eV; see, e.g., Warneck 1962) has been added to the system. With this addition, both UV photolysis and proton bombardment of ices are now possible, merely by turning the ice sample to face the appropriate energy source.

The UV lamp system is similar to that used by others (e.g., Allamandola et al. 1988; Gerakines et al. 1996) and is separated from the vacuum by a UV-transmitting ($\lambda > 104$ nm) lithium fluoride window. We calculated the lamp's flux at the ice to be $\phi_{UV} = 8.6 \times 10^{13}$ photons $\text{cm}^{-2} \text{s}^{-1}$ (for $\lambda < 185$ nm) by measuring the $\text{O}_2 \rightarrow \text{O}_3$ conversion rate in the photolysis of a pure O_2 ice at 18 K. This method of UV flux measurement is well-documented for gas-phase O_3 production (e.g., Warneck 1962). Due to the lack of solid O_3 data, we have assumed gas-phase values for both the O_3 quantum yield (1.92; Groth 1937), and the strength of the O_3 stretching mode at 1030 cm^{-1} ($A = 1.4 \times 10^{-17} \text{ cm molecule}^{-1}$; Smith et al. 1985). Given these assumptions, the flux estimate is accurate to within a factor of two.

Depending on the experiment, ice thicknesses ranged from 0.1 to more than $2 \mu\text{m}$ and were typically condensed at rates of about 2.8 to 4.7×10^{15} molecules $\text{cm}^{-2} \text{s}^{-1}$ (3 to $5 \mu\text{m hr}^{-1}$). Except in special cases, UV experiments were performed on samples less than $0.5 \mu\text{m}$ thick to ensure UV penetration into the bulk of the ice, since the optical depth for a UV photon in an H_2O ice, or the depth to which the UV transmission drops to 37%, is $0.15 \mu\text{m}$. This assumes $\rho = 1 \text{ g cm}^{-3}$ and a UV absorption cross-section of $2 \times 10^{-18} \text{ cm}^2$ from Okabe (1978). The UV absorption by CO_2 is about five to more than ten times lower than that of H_2O from 110 to 160 nm (Okabe 1978), and

therefore the amount of H_2O was the limiting factor in choosing appropriate ice thicknesses for the UV experiments.

To process the ice by proton bombardment, the ice sample is rotated to face a beam of 0.8 MeV protons generated by a Van de Graaff accelerator. At this energy, protons can pass through ices up to $20 \mu\text{m}$ thick. To photolyze with UV, the mirror is rotated to face the UV lamp. Three methods of photolysis were used: (1) condensation of a single ice layer, with subsequent photolysis, (2) photolysis of several layers, each condensed atop the last, and (3) simultaneous condensation and photolysis, where gases are passed through a secondary deposition tube (shown in Fig. 1) positioned to release them while the mirror is facing the UV lamp. Gases in experiments using method (3) were condensed at a rate of about 3.3×10^{14} molecules $\text{cm}^{-2} \text{s}^{-1}$ ($0.35 \mu\text{m hr}^{-1}$).

Radiation doses in the proton irradiation experiments were calculated using the average stopping powers and molecular densities for each given ice sample, as described in detail by Moore & Hudson (1998). Doses in such experiments are typically given in units of energy per 18 amu of reactant, but in photolysis experiments, levels of processing are usually expressed in terms of the total UV exposure time. Conversion to energy dose per 18 amu of reactant, D , is possible when an ice film is condensed to a column density of N and subsequently photolyzed for a time t with a photon flux of ϕ_{UV} :

$$D = 18 \frac{\phi_{UV} t E_{h\nu}}{m N}, \quad (1)$$

where $E_{h\nu}$ is the average energy per UV photon and m is the average molecular mass of reactant in amu. It is assumed that the ice is optically thin and that the UV penetrates the entire ice sample. This calculation is not straightforward for ices that are simultaneously condensed and photolyzed, since the number of reactant molecules is constantly increasing over the course of the experiment.

3. Results

3.1. Comparison of spectra

We have formed H_2CO_3 by both proton bombardment and UV photolysis of $\text{H}_2\text{O}:\text{CO}_2$ ice mixtures. Fig. 2a shows the mid-IR spectrum of an $\text{H}_2\text{O}:\text{CO}_2 = 1$ ice at 18 K (with a thickness of $2.08 \mu\text{m}$) before and after proton irradiation to a dose of $48 \text{ eV (18 amu)}^{-1}$, and of the same ice after warming to 250 K to evaporate the volatile components and leave only H_2CO_3 . Fig. 2b contains spectra of an $\text{H}_2\text{O}:\text{CO}_2 = 1$ mixture after simultaneously condensing and photolyzing as described in Sect. 2 for 3 hr, and after warming the processed ice to 250 K. Low-temperature spectra in Fig. 2 (*i* and *ii*) have been normalized to the height of the H_2O 3250 cm^{-1} ($3.1 \mu\text{m}$) feature, and high-temperature spectra (*iii*) have been normalized to the height of the H_2CO_3 1508 cm^{-1} ($6.6 \mu\text{m}$) feature. The four most intense absorptions in pure H_2CO_3 at 250 K fall at 2620, 1714, 1507, and 1298 cm^{-1} , and all are present in the low-temperature $\text{H}_2\text{O}:\text{CO}_2$ irradiated ice spectra shown in Fig. 2(*ii*).

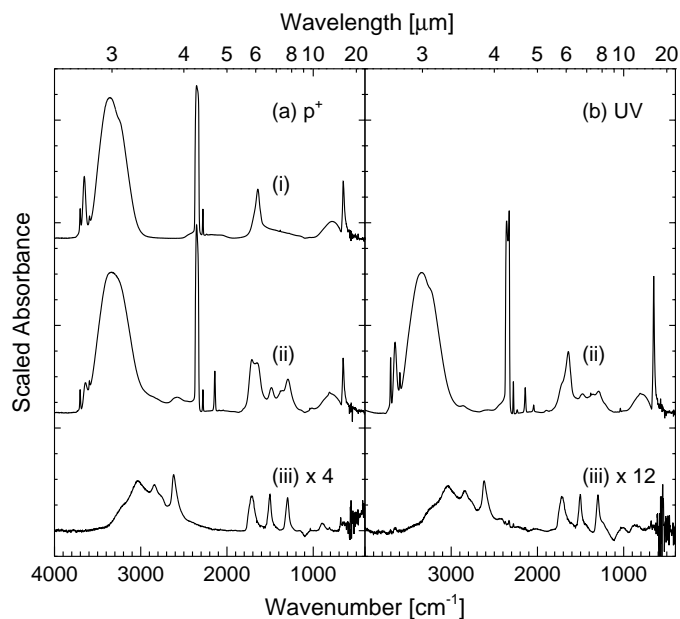


Fig. 2a and b. Spectra of an H₂O:CO₂ = 1 ice over the course of two experiments with different processing methods: **a** Proton irradiation and **b** simultaneous condensation and UV photolysis. Spectra were taken before processing at 18 K (*i*, irradiation case only), after processing (*ii*), and after heating the processed ice to 250 K (*iii*). Spectra in (*i*) and (*ii*) have been normalized to the H₂O 3250 cm⁻¹ (3.1 μm) band, and spectra in (*iii*) to the H₂CO₃ 1508 cm⁻¹ (6.6 μm) band

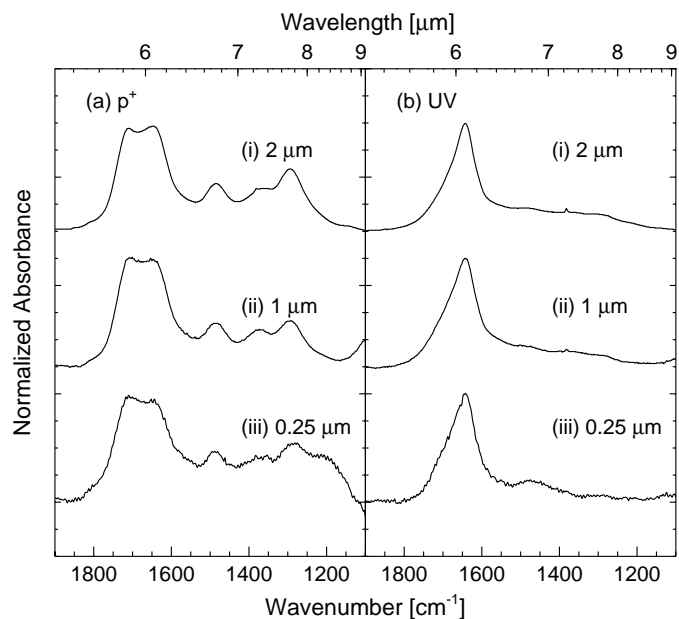


Fig. 3a and b. 1800–1200 cm⁻¹ (5.6 to 8.3 μm) region of **a** proton-irradiated and **b** UV-photolyzed ices at 18 K with varying initial ice thicknesses. (*i*) 0.25 μm, (*ii*) 1 μm, (*iii*) 2 μm. All spectra have been normalized to the height of the H₂O band at 1640 cm⁻¹ (6.1 μm). Below 1200 cm⁻¹, the spectra (especially in *iii*) are affected by an artifact created by the incomplete ratioing of a background feature

In Fig. 3, we compare proton- and UV-processed H₂O:CO₂ ice spectra at 18 K in the 2000–1000 cm⁻¹ (5–10 μm) region for different starting thicknesses. Spectra are normalized to the height of the H₂O bending mode at 1640 cm⁻¹ (6.1 μm). In the case of proton irradiation (Fig. 3a), the profiles in each case are identical, verifying that the net conversion of H₂O + CO₂ → H₂CO₃ does not depend on the starting thickness of the ice within the range of these experiments (total dose = 48 eV (18 amu)⁻¹). Protons of this energy (0.8 MeV) can process the entire bulk of ices with thicknesses up to 20 μm. The size of the H₂CO₃ features relative to those of H₂O in our proton-irradiated H₂O:CO₂ ices are independent of the initial ice's thickness (from 0.25 to 2 μm), but this is not the case for photolyzed ices.

In the UV cases, (Fig. 3b), total photolysis times were about 3 hr, but the sizes of the H₂CO₃ bands produced relative to the H₂O bending mode at 1660 cm⁻¹ are smaller in ices with greater initial thicknesses. This result is not surprising, given the UV optical depth of 0.15 μm mentioned above.

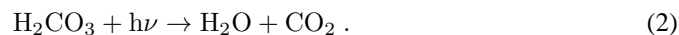
Since UV photons process the top layer of an ice and do not penetrate it completely, the features of new products in thicker ices are observed against the IR spectrum of the unprocessed ice beneath. Fig. 4(*i*) shows the spectrum of an H₂O:CO₂ ice, initially 1 μm in thickness, that was photolyzed for 1 hr. Two different techniques were used to demonstrate that by increasing the amount of UV exposure in the bulk of the ice, H₂CO₃ features can be enhanced. First, experiments were performed in which photolyzed layers were built up on top of each other.

Each 0.26 μm layer of an H₂O:CO₂ = 1 mixture was photolyzed for 1 hr. Four layers were used to create the final processed ice sample whose spectrum is shown in Fig. 4(*ii*). Second, an ice was simultaneously photolyzed and condensed at a rate of 0.35 μm hr⁻¹ to a total thickness of ≈ 1 μm (Fig. 4(*iii*)). The most intense signatures of H₂CO₃ were obtained in the experiment involving simultaneous photolysis and condensation.

Anion formation (either CO₂⁻ or OH⁻) is thought to be the key to the H₂CO₃ production, and so we performed an experiment that included 1 % sulfur hexafluoride (SF₆), an electron scavenger which would consume any available electrons and inhibit the formation of OH⁻ and CO₂⁻. The yield of H₂CO₃ dropped significantly when SF₆ was added to the ice in the irradiation experiments. However, when it was added to the H₂O:CO₂ ice in a UV photolysis experiment, the H₂CO₃ abundance did not drop significantly. The reason for this discrepancy is unclear, but it is likely that the combination of broad H₂CO₃ features and low abundance of H₂CO₃ produced in the UV case (without any SF₆) makes the difference difficult to detect.

3.2. Measurement of H₂CO₃ intrinsic IR band strengths

We have employed a technique to determine the band strengths of a molecule by photodissociation into a product with known strengths. In this section, we present the results of band strength measurements by photodissociation of pure H₂CO₃ into H₂O and CO₂ as follows:



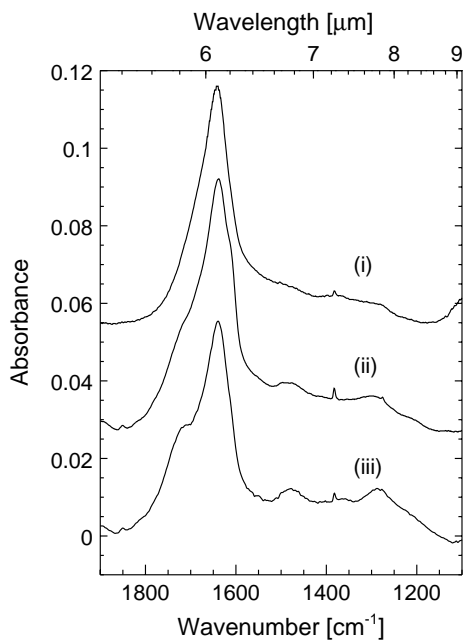


Fig. 4. H₂O:CO₂ = 1 ices after UV photolysis at 18 K. (i) Ice condensed to 1 μm in thickness before photolysis for 1 hr; (ii) four 0.26 μm layers, each condensed on the last and photolyzed for 1 hr; (iii) simultaneous UV and condensation to ≈ 1 μm at a rate of 0.35 μm hr⁻¹

Therefore the number of CO₂ molecules produced equals the number of H₂CO₃ molecules destroyed. CO must also be taken into account once significant amounts are created from the CO₂, and this occurred in our experiments at energy doses greater than 22 eV (18 amu)⁻¹.

Since the intrinsic IR band strengths of CO and CO₂ have already been determined (pure CO: Jiang et al. 1975; pure CO₂: Yamada & Person 1964; water-dominated mixtures with CO and CO₂: Gerakines et al. 1995), we can calculate column densities for CO₂ and CO at any stage in the photolysis from the CO₂ band at 2342 cm⁻¹ (4.27 μm) and the CO band at 2140 cm⁻¹ (4.67 μm). For these calculations, we have used band strengths of $A(\text{CO}_2, 2342 \text{ cm}^{-1}) = 7.6 \times 10^{-17} \text{ cm molecule}^{-1}$ and $A(\text{CO}, 2140 \text{ cm}^{-1}) = 1.1 \times 10^{-17} \text{ cm molecule}^{-1}$ (Gerakines et al. 1995 showed that these values are independent of ice mixture). For each H₂CO₃ IR feature, we may then divide the loss of H₂CO₃ absorption area by the gain in CO₂ and CO column densities, yielding the absorption per unit column density, or intrinsic IR band strength (in units of [cm⁻¹]/[molecule cm⁻²] = [cm molecule⁻¹]).

Two experiments were performed, with different initial H₂CO₃ thicknesses and total photolysis times. In each case, the H₂CO₃ was produced by the irradiation of an H₂O:CO₂ = 1 ice, followed by warming to 250 K and re-cooling to 18 K (spectra not shown). Then the remaining H₂CO₃ was photolyzed at 18 K by the UV lamp to create H₂O and CO₂ as in Eq. (2). Initial H₂O:CO₂ ice thicknesses for the two experiments were 2.08 and 5.20 μm, respectively, and total photolysis times were 90 and 180 min, respectively.

Table 1. Band strengths of annealed H₂CO₃ at 18 K

Position [cm ⁻¹]	Vibrational Mode ^a	Band Strength, <i>A</i> [10 ⁻¹⁷ cm molecule ⁻¹]
2840+2761	O-H stretch	9.8 ± 0.4
2626	O-H stretch	16.0 ± 0.8
1719	C=O stretch	11 ± 1 ^b
1508	C-OH asym stretch	6.5 ± 0.6
1307	C-OH i.p. bend	10 ± 2
1038	C-OH sym stretch	0.14 ± 0.02
908	C-OH o.p. bend	5.6 ± 0.8
813	CO ₃ o.p. bend	? ^c
690	CO ₃ i.p. bend	1.3 ± 0.2

^a Band assignments from DelloRusso et al. 1993; “asym” = asymmetric, “sym” = symmetric, “i.p.” = in-plane, “o.p.” = out-of-plane;

^b derived by scaling the strength of the 1508 cm⁻¹ band (see text);

^c unable to determine

Areas of nine IR bands of H₂CO₃ are plotted in Fig. 5 as functions of the CO₂+CO column densities during the photolyses. Linear least-square fits to each band’s data are also shown, and the intrinsic IR band strength is given by the slope of the fit (listed in Table 1). Data points in Fig. 5 representing the shorter experiment (open circles) have been shifted upwards for fitting purposes. In the longer experiment (solid squares), the trend becomes obviously non-linear for most bands after about 40 min of photolysis (corresponding to $N_{\text{CO}_2} + N_{\text{CO}} > 1 \times 10^{16} \text{ cm}^{-2}$). This is likely caused by the combination of three effects: the amorphization of H₂CO₃ by the photolysis, the growth of H₂O bands underneath those of H₂CO₃, and the decomposition of CO₂ into something not taken into account. For this reason, fits were made using only the first 30 min of photolysis data from the longer experiment in combination with all data from the shorter experiment. With the exception of the 813 cm⁻¹ band of H₂CO₃, clear band strength estimates could be made and are listed in Table 1. Band positions listed are those observed in the annealed H₂CO₃ at 18 K, and differ slightly from those found in Moore & Khanna (1991) and DelloRusso et al. (1993) for H₂CO₃ at 250 K, since band positions are temperature-dependent. The 2841 cm⁻¹ band observed in H₂CO₃ at 250 K splits into two bands when cooled to 18 K, and the new pair of features are listed in Table 1 and Fig. 5 as “2840+2761”.

Although the evolution of the 1719 cm⁻¹ band is extremely well fit by a straight line in Fig. 5, its rate of decrease due to photodissociation is slower than that of the other H₂CO₃ bands (excluding the 813 cm⁻¹ band, which does not seem to decrease at all). After the first 30 min of photolysis, its area drops by only 11 %; all other bands lose 21 to 35 % of their initial areas during this time. If the H₂CO₃ is merely breaking down into H₂O and CO₂, all of its bands should shrink at the same rate. Therefore, the slope of the linear fit to the 1719 cm⁻¹ band underestimates its true band strength. This is most likely caused by the growth of the underlying H₂O bending mode at 1660 cm⁻¹ (6 μm) or a process more complex than the simple dissociation of H₂CO₃ (e.g., changes in intermolecular bonding or the formation of other products such as H₂CO). For this reason, we have used

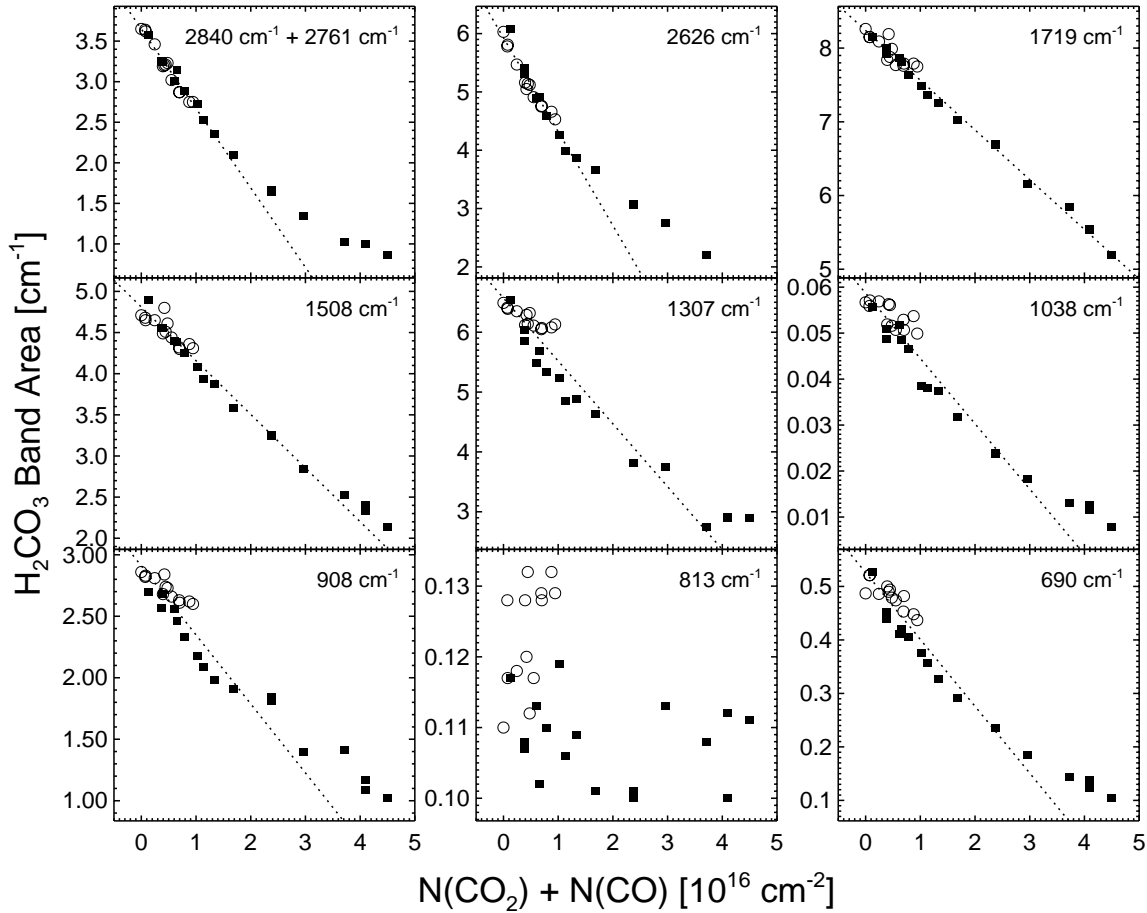


Fig. 5. Areas (in cm^{-1}) of the H_2CO_3 IR bands (denoted by position in cm^{-1}) vs. the combined column densities of CO_2 and CO (in 10^{16}cm^{-2}) during the photolysis of annealed H_2CO_3 in two experiments (solid squares and open circles). Dotted lines represent the best linear least-square fits to all data in the shorter experiment plus the first 30 min of data in the longer experiment

the value for the 1508cm^{-1} band in any calculations requiring the abundance of H_2CO_3 . However, scaling the calculated strength of the 1508cm^{-1} band by the ratio of initial 1719 and 1508cm^{-1} band areas gives a 1719cm^{-1} band strength of $(1.1 \pm 1) \times 10^{-16} \text{cm molecule}^{-1}$ (almost twice the slope of the fit in Fig. 5). This value is listed in Table 1, where the error bar represents the 10 % variation in the ratio of 1719 to 1508cm^{-1} band areas over the first 30 min of photolysis.

3.3. Calculation of formation and destruction rates

Production rates in ion irradiation experiments are usually given in terms of the yield, G , the number of molecules produced by an absorbed energy of 100eV . In photolysis experiments, results are usually expressed in terms of a formation cross-section, σ_f (in cm^2). Assuming zeroth-order kinetics,

$$\frac{dN_P}{dt} = \sigma_f \phi_{\text{UV}} N_R^0, \quad (3)$$

where N_P is the column density of product molecules formed, ϕ_{UV} is the UV flux, and N_R^0 is the initial reactant column density. Integrating gives

$$N_P = (\sigma_f \phi_{\text{UV}} N_R^0) t, \quad (4)$$

so that a plot of N_P vs. t gives σ_f , as ϕ_{UV} and N_R^0 are known. To facilitate comparisons between proton irradiation and UV photolysis experiments, we convert UV formation cross-sections to formation yields. Since the yield is the ratio of product molecules to input energy absorbed ($\times 100$), we may calculate G_{UV} using

$$\begin{aligned} G_{\text{UV}} &= 100 \times \frac{\text{products cm}^{-2}}{\text{energy absorbed cm}^{-2}} \\ &= 100 \frac{N_P}{\phi_{\text{UV}} t E_{h\nu}}, \end{aligned} \quad (5)$$

where t is the elapsed photolysis time, $E_{h\nu}$ is the average energy per UV photon, and it is assumed that all incident photons are absorbed by the ice. Eq. (5) may be re-written in terms of the formation cross-section by substituting the right-hand side of Eq. (4) for N_P :

$$G_{\text{UV}} = 100 \frac{N_R^0 \sigma_f}{E_{h\nu}}. \quad (6)$$

We will denote yields in proton irradiation experiments by G_{p+} , and those in UV photolysis experiments by G_{UV} . Results are summarized in Table 2. Yields of CO_2 destruction are denoted

Table 2. Yields in H₂O:CO₂ = 1 processing experiments at 18 K

Species	G_{p+}	G_{UV}
H ₂ CO ₃	0.028 ± 0.024	0.030 ± 0.016
CO	0.20 ± 0.07	0.32 ± 0.15
CO ₂	-0.55 ± 0.05	-0.56 ± 0.09

by negative values of G in Table 2, and were measured using the area of the ¹³CO₂ band near 2280 cm⁻¹ (4.39 μm) and assuming a ratio of ¹²CO₂/¹³CO₂ = 87. Destruction rates for H₂CO₃ in the H₂O:CO₂ ice mixtures at 18 K were not measured since a linear production rate, without reaching an equilibrium between reactants and product, is seen throughout the course of these experiments.

Fig. 6 contains plots of CO and H₂CO₃ column densities during the processing of an H₂O:CO₂ = 1 ice at 18 K as functions of energy absorbed per unit area (given in units of 10¹⁸ eV cm⁻²). Data points shown represent three different experiments for both proton irradiation and UV photolysis. Since the strengths of the H₂CO₃ bands in a mixture of H₂O:CO₂:H₂CO₃ at 18 K are not known, we have calculated a strength by scaling the 1508 cm⁻¹ band in pure H₂CO₃ at 18 K (measured in Sect. 3.2). The scaling factor was determined from the ratio of the 1508 cm⁻¹ band area in a pure H₂CO₃ sample at 18 K and that of the same band in the H₂O:CO₂:H₂CO₃ ice (at 18 K) from which the pure H₂CO₃ sample was produced (by annealing to remove H₂O and CO₂ as described in Sect. 3.2). In a mixture of H₂O:CO₂:H₂CO₃ at 18 K, this band falls at 1485 cm⁻¹, and the strength was calculated to be $A = 5.9 \times 10^{-17}$ cm molecule⁻¹. All values of $N_{\text{H}_2\text{CO}_3}$ in Fig. 6 have been calculated with this band strength, where the 1485 cm⁻¹ band was fit by a gaussian curve with a linear baseline from about 1530 to 1150 cm⁻¹ (to approximate the wing of the 1640 cm⁻¹ H₂O ice band).

Values of G_{p+} given in Table 2 and Fig. 6a were calculated from the combined data of four proton irradiation experiments. The average ratio of product column density to energy absorbed per unit area give $G_{p+}(\text{CO}) = 0.20 \pm 0.07$ and $G_{p+}(\text{H}_2\text{CO}_3) = 0.028 \pm 0.024$ (the data in Fig. 6 are plotted on logarithmic scales for comparison purposes). The large uncertainty in $G_{p+}(\text{H}_2\text{CO}_3)$ is due to the fact that there is a high degree of scatter in $N_{\text{H}_2\text{CO}_3}$. Data points appear to cluster into two major groups, positioned in the lower center and upper right regions of Fig. 6a. Points in the low-center region represent results from two ices with thicknesses of about 0.75 μm, whereas the those in the upper-right region represent ices with thicknesses of about 2 and 5.5 μm. Future laboratory work should investigate a possible dependence of $G_{p+}(\text{H}_2\text{CO}_3)$ on ice thickness.

This value of H₂CO₃ yield (0.028) is about a factor of 10 lower than those previously published, where band strengths were estimated assuming a mass density of 1 g cm⁻³ and the change in H₂CO₃ band area relative to the ice's thickness during sublimation at 250 K (e.g., DelloRusso et al. 1993). They are also lower than those obtained by Brucato et al. (1997), who derived H₂CO₃ band strengths by ion-implantation into pure

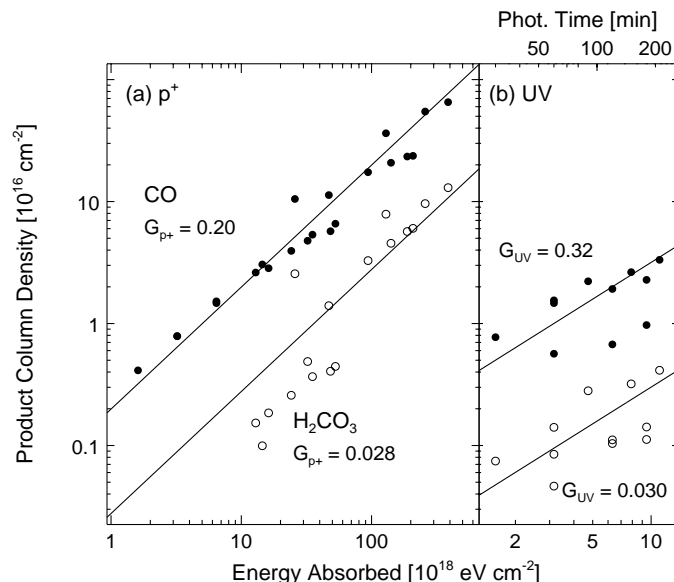


Fig. 6a and b. Combined results of three proton irradiation experiments **a** and three UV photolysis experiments **b**. Column densities of CO (solid circles) and H₂CO₃ (open circles) are plotted vs. total energy absorbed per unit area. Photolysis time is given in the top axis of **b**. The slope of the trend in each case, given by the solid lines, represents the formation yield (G_{p+} or G_{UV}) as calculated from the average over all data points

CO₂ and assuming all ions formed H₂CO₃. The growth of the H₂CO₃ features during formation does not level off, even at the highest energy doses in these experiments (48 eV (18 amu)⁻¹).

The growth of CO and H₂CO₃ column densities during the corresponding photolysis experiments are plotted in Fig. 6b. Photolysis time is given by the top x-axis. Ices were condensed and subsequently photolyzed. Average ratios of N_{CO} and $N_{\text{H}_2\text{CO}_3}$ to the energy absorbed per unit area ($= \phi_{UV} E_{h\nu} t$) give yields of $G_{UV}(\text{CO}) = 0.32 \pm 0.15$ and $G_{UV}(\text{H}_2\text{CO}_3) = 0.030 \pm 0.016$. This calculation assumes all photon energy was absorbed in the three ice samples studied, whose thicknesses were 1.04, 1.04 and 2.08 μm. Using Eq. (6), these values of G_{UV} correspond to formation cross-sections of $\sigma_f(\text{CO}) = (1.1 \pm 0.5) \times 10^{-19}$ cm² and $\sigma_f(\text{H}_2\text{CO}_3) = (1.1 \pm 0.6) \times 10^{-20}$ cm², respectively (using $N_{\text{H}_2\text{O}} + N_{\text{CO}_2}$ as the initial reactant abundance and assuming that all energy is absorbed in the top 0.20 μm of the ice).

It is clear from the values of G listed in Table 2 that CO and H₂CO₃ do not account for all of the carbon-bearing molecules formed from the original CO₂. The formyl radical, HCO, was identified in these experiments by its band near 1850 cm⁻¹ (5.4 μm). Although highly variable, its formation yield was about $G = 0.001$ in all experiments (assuming a band strength of 2.1×10^{-17} cm molecule⁻¹ from Hudson & Moore 1999). The CO₃ molecule was also formed in these irradiation and photolysis experiments, identified by its absorption feature at 2045 cm⁻¹ (4.9 μm; see Jacox & Milligan 1971). However, no formation rates or yields could be calculated since the CO₃ band strength is not known. It is possible that other molecules such

as H₂CO form during processing, but their absorption bands are masked by the stronger features of H₂O and H₂CO₃ in the IR spectra.

We also calculated the photodissociation cross-section and destruction yield for crystalline H₂CO₃ from the photolysis experiments used to determine its IR band strengths in Sect. 3.2. Since the ice is optically thin, the dissociation follows as a zeroth-order reaction, and the abundance of carbonic acid should drop linearly with photolysis time, e.g.,

$$N_{\text{H}_2\text{CO}_3}^t = N_{\text{H}_2\text{CO}_3}^0 (1 - \sigma_{\text{pd}} \phi_{\text{UV}} t), \quad (7)$$

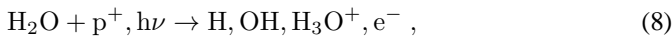
where $N_{\text{H}_2\text{CO}_3}^0$ is the initial abundance of H₂CO₃, and σ_{pd} is the cross-section for H₂CO₃ photodissociation. A fit in the form of Eq. (7) to the first 25 min of photolysis data for the 1508 cm⁻¹ band of H₂CO₃ yields $\sigma_{\text{pd}} = (1.3 \pm 0.3) \times 10^{-18}$ cm². The formation cross-section of CO₂ from crystalline H₂CO₃ in this experiment was measured to be $\sigma_{\text{f}} = (3.16 \pm 0.14) \times 10^{-20}$ cm². An experiment was also performed where crystalline H₂CO₃ at 18 K was irradiated by 0.8 MeV protons. In this case, a fit to data points at low doses (from 0 to 1.28 eV (18 amu)⁻¹) gives $G_{\text{p}+}(-\text{H}_2\text{CO}_3) = 4.2 \pm 0.3$, and $G_{\text{p}+}(\text{CO}_2) = 2.4 \pm 0.2$.

Since the H₂CO₃ samples in the photolysis experiments were optically thin to UV, not all photons were absorbed, and we cannot convert cross-sections to yields in these experiments with Eq. (6). However, we can work backwards, using Eq. (6) to convert the measured $G_{\text{p}+}$ values to “cross-sections” for the sake of comparing them with the results of the photolysis experiments. In this case, we find that irradiation destroys the crystalline H₂CO₃ 37 times faster and forms CO₂ 875 times faster than photolysis.

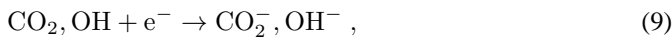
4. Discussion

4.1. Reaction schemes

The chemical evolution of the processed H₂O:CO₂ ice is thought to proceed along the following path: first, the direct dissociation of H₂O–



where products such as H₂, H₂O₂, and HO₂ may be formed by reaction of the primary dissociation products. The next step is the formation of CO₂⁻ and/or OH⁻, which quickly react to form bicarbonate:



and/or



Finally, bicarbonate reacts with a positive ion to form H₂CO₃:



Secondary electrons are produced in ion-irradiated ices as discussed in Spinks & Woods (1990), but their production in

photolyzed ices (Eq. 8) is not widely discussed. However, Baron et al. (1978) have shown that the photoelectric threshold of amorphous water ice at 13 K is 8.7 eV. We therefore consider electron production in our UV-photolyzed ices reasonable. In our experiments, these electrons are trapped by the CO₂ and OH by forming the bicarbonate ion (which then goes on to form H₂CO₃). The importance of electron transfer in this reaction scheme (Eqs. 9–11) was confirmed by the addition of SF₆ in the ice mixture (see Sect. 3.1). The reaction given by Eq. (12) may be impeded by the presence of an H⁺ scavenger such as NH₃.

4.2. Astrophysical significance

These results have significance over a large range of astrophysical environments, from icy grain mantles in the interstellar medium, (thickness ≈ 0.01 – 0.1 μm), to ices on the surfaces of planetary bodies (1 μm – several mm) and in cometary nuclei (1 m – several km).

The dominant source of energetic processing for an icy mixture in different astrophysical regimes depends on the nature of the radiation environment and the thickness of the ice layer found there. Interstellar icy grain mantles are subjected to two sources of processing: UV Lyman- α photons and cosmic rays. In cold dark clouds, models show that an ice layer absorbs nearly equal doses from each source (see review by Moore 1999 and references therein). In cold diffuse clouds, however, the UV photon flux dominates, where a UV dose of 5×10^3 eV molecule⁻¹ is absorbed in a 0.1 μm ice layer after 10⁵ yr, as compared to < 1 eV molecule⁻¹ from low-energy cosmic-ray protons (see Moore 1999). Processing of cometary ices stored for 4.6 Gyr in the Oort cloud is dominated by cosmic rays, and it is estimated that 41 eV molecule⁻¹ is deposited in the upper 20 cm of ice from cosmic-ray protons. Deeper layers accumulate smaller doses, but the upper layers of dynamically new comets are evaporated at each apparition, so older comets may process and evaporate once-deep layers. However, the contribution of products from UV photons is insignificant in the case of observed Oort-cloud comets, since the photon penetration depth is small compared to the thickness of evaporated cometary ice layers at each apparition (0.15 μm vs. several meters). The surfaces of the Galilean satellites experience a constant flux of energetic ions (mainly from the Jovian magnetosphere) along with Solar UV photons. Although Europa receives the highest particle flux, the other satellites receive enough radiation to drive ice processing as well. The average UV flux density in the Jovian system is $< 1\%$ that of the energetic particles (see Carlson et al. 1999 and references therein), and the contribution of UV photons to the abundance of observed molecules in these environments is also insignificant, since IR observations of the Galilean satellites sample the top ~ 50 μm of the ice (vs. the UV penetration depth of 0.15 μm).

Our results indicate that whenever H₂O:CO₂ icy mixtures are processed (either by UV photons or cosmic-ray particles as described above), CO and H₂CO₃ will be formed. The lack of H₂O:CO₂ photolysis data before this study is likely due to the fact that no products other than CO are formed above

the 1 % level on time scales appropriate to interstellar conditions. Given that the cosmic-ray-induced UV flux inside dark clouds amounts to $\sim 10^3 \text{ cm}^{-2} \text{ s}^{-1}$ (Prasad & Tarafdar 1983), about $5 \times 10^8 \text{ yr}$ (or 50 times the expected lifetime of a molecular cloud) would be required to form 1 % H₂CO₃ relative to CO₂ (a reasonable detection limit). The Galactic cosmic-ray flux absorbed by an icy grain mantle is $\sim 10^3 \text{ eV cm}^{-2} \text{ s}^{-1}$ in cold dense clouds (Moore 1999), and therefore a formation yield of 0.028 (Table 2) also requires $\sim 10^8 \text{ yr}$ to generate a 1 % abundance of H₂CO₃ relative to CO₂. In the case of the quiescent cloud medium toward the background field star Elias 16, the expected H₂CO₃ column density could be as much as $4.6 \times 10^{16} \text{ cm}^{-2}$ (1 % of the CO₂ or 0.2 % of the total H₂O in this line of sight; Whittet et al. 1998).

After 4.6 Gyr (and $41 \text{ eV molecule}^{-1}$), the top 20 cm of Oort-cloud comet ice would generate an H₂CO₃:CO₂ ratio of about 1 % as well. H₂CO₃ production should also occur in the high-radiation environment of the icy Galilean satellites such as Europa. The total average energy flux at Europa is $5 \times 10^{13} \text{ eV cm}^{-2} \text{ s}^{-1}$ for energetic particles (Carlson et al. 1999), and hence $1.5 \times 10^{10} \text{ H}_2\text{CO}_3 \text{ molecules cm}^{-2} \text{ s}^{-1}$ could be formed there by an H₂O:CO₂ ice on its surface. See Delitsky & Lane (1998) for a review of Galilean ice chemistry.

H₂CO₃ is less volatile than H₂O and CO₂, therefore it may remain on the surface of an icy satellite or in a comet's crust after H₂O and CO₂ have evaporated. It is also an acid, which could play a role in low-temperature acid-base reactions there. However, as shown in Sect. 3.3, the destruction rate of pure crystalline H₂CO₃ is about 500–1000 times faster than its formation rate inside an H₂O:CO₂ mixture. With this in mind, areas of pure H₂CO₃ will probably be sustained only if they are protected from direct exposure to processing.

5. Summary

We have shown that H₂CO₃ is formed in both the UV photolysis and proton irradiation of H₂O:CO₂ = 1 ice mixtures at 18 K (Fig. 2). After long photolysis times, signatures of H₂CO₃ are apparent, but no clear evidence for H₂CO was found.

Formation yields of H₂CO₃, and CO in H₂O:CO₂ = 1 ices at 18 K are listed in Table 2. Intrinsic strengths have been measured for eight IR bands of H₂CO₃ (Fig. 5, Table 1) by converting H₂CO₃ into CO₂, a molecule with well-known IR band strengths. Yields of H₂CO₃ destruction and CO₂ formation in the processing of annealed H₂CO₃ at 18 K were also measured. It is likely that H₂CO₃ will exist in astrophysical environments in low abundance, most easily observed in cometary nuclei or on the surfaces of icy Galilean satellites such as Europa.

Acknowledgements. This work was performed while P.A.G. held an NRC-NASA/GSFC Research Associateship. This work was supported by NASA through RTOPs 344-33-01 and 344-02-57. Claude Smith and Steve Brown of the NASA/Goddard Radiation Facility are thanked for assistance with the proton irradiations.

References

- Allamandola L.J., Sandford S.A., Valero G.J., 1988, *Icarus* 76, 225
 Baron B., Hoover D., Williams F., 1978, *J. Chem. Phys.* 68, 1997
 Bockelée-Morvan D., 1997, In: van Dishoeck E.F. (ed.) *Molecules in Astrophysics: Probes and Processes*. Kluwer, Dordrecht, p. 218
 Brucato J.R., Palumbo M.E., Strazzulla G., 1997, *Icarus* 125, 135
 Carlson R.W., Anderson M.S., Johnson R.E. et al., 1999, *Sci* 283, 2062
 Crovisier J., 1998, *Faraday Discussion* 109, 437
 Delitsky M.L., Lane A.L., 1998, *J. Geophys. Res.* 103 (13), 31391
 DelloRusso N., Khanna R.K., Moore M.H., 1993, *J. Geophys. Res.* 98, 5505
 Gerakines P.A., Schutte W.A., Ehrenfreund P., 1996, *A&A* 312, 289
 Gerakines P.A., Schutte W.A., Greenberg J.M., van Dishoeck E.F., 1995, *A&A* 296, 810
 Gerakines P.A., Whittet D.C.B., Ehrenfreund P. et al., 1999, *ApJ* 522, 357
 Groth W., 1937, *Z. Phys. Chem.* 37, 307
 Herr K.C., Pimentel G.C., 1969, *Sci* 166, 496
 Hudson R.L., Moore M.H., 1995, *Radiat. Phys. Chem.* 45, 779
 Hudson R.L., Moore M.H., 1999, *Icarus* 140, 451
 Jacox M.E., Milligan D.E., 1971, *J. Chem. Phys.* 54, 919
 Jiang G.J., Person W.B., Brown K.G., 1975, *J. Chem. Phys.* 64, 2101
 Larson H.P., Fink U., 1972, *ApJ* 171, L91
 McCord T.B., Hansen G.B., Clark R.N. et al., 1998, *J. Geophys. Res.* 103, 8603
 Moore M.H., 1999, In: d'Hendecourt L., Joblin C., Jones A. (eds.) *Solid Interstellar Matter: the ISO Revolution*. Springer-Verlag, New York, p. 199
 Moore M.H., Hudson R.L., 1998, *Icarus* 135, 518
 Moore M.H., Khanna R.K., 1991, *Spectrochim. Acta* 47A, 255
 Okabe H., 1978, *Photochemistry of Small Molecules*. Wiley, New York
 Prasad S.S., Tarafdar S.P., 1983, *ApJ* 267, 603
 Quirico E., Douté S., Schmitt B. et al., 1999, *Icarus* 139, 159
 Smith M.A.H., Rinsland C.P., Fridovich B., Rao K.N., 1985, In: Rao K.N. (ed.) *Molecular Spectroscopy: Modern Research*. Vol. III, Academic Press, London, p. 111
 Spinks J.W.T., Woods R.J., 1990, *An Introduction to Radiation Chemistry*. 3rd ed., Wiley, New York
 Warneck P., 1962, *Applied Optics* 1 (6), 721
 Whittet D.C.B., Schutte W.A., Tielens A.G.G.M. et al., 1996, *A&A* 315, L357
 Whittet D.C.B., Gerakines P.A., Tielens A.G.G.M. et al., 1998, *ApJ* 498, L159
 Yamada H., Person W.B., 1964, *J. Chem. Phys.* 41, 2478
 Zhao N.-S., 1990, Ph.D. Thesis, Chapter 4, Leiden University, the Netherlands